Capping nanoparticles with graphene quantum dots for enhanced thermoelectric performance†

Yuantong Liang,[ab] Chenguang Lu,*[a] Defang Ding,[a] Man Zhao,[a] Dawei Wang,[a] Chao Hu,[c] Jieshan Qiu,[c] Gang Xie*[b] and Zhiyong Tang*[a]

Graphene quantum dots (GQDs) are shown to serve as phase transfer agents to transfer various types of nanoparticles (NPs) from non-polar to polar solvents. Thorough characterization of the NPs proves complete native ligand exchange. Pellets of this GQD–NP composite show that the GQDs limit the crystal size during spark plasma sintering, yielding enhanced thermoelectric performance compared with NPs exchanged with inorganic ions. A photoluminescence study of the GQD–NP composite also suggests energy transfer from GQDs to NPs.

Introduction

Inorganic nanoparticles (NPs) have many unique properties that have attracted much attention since their introduction.[1] However, the most versatile wet-chemistry synthetic methods for producing NPs inevitably coat them with long chain organic ligands, which insulate the NPs from each other and their environment. Removal of such organic coatings thus becomes a key challenge for incorporating NPs into devices as functional parts. Many agents have been proposed to replace the native ligands, including inorganic anions,[2–4] chalcogenide complexes,[5,6] NOBF₄,[7] Meerwein's salt,[8] formic acid,[9,10] thiolate ligands,[11–14] and polymers.[15,16] These agents effectively strip the NPs of their native ligands and bring them closer together, improving electrical conductivity and energy transfer. However, these native ligand exchangers, except for metal chalcogenide complexes and polymers, are mostly small chemical species and serve as stabilizing agents only.

Recent advances in nanocomposite materials allow for a scalable methodology to generate multifunctional materials with properties stemming from both their individual components and, more interestingly, their synergistic interactions.[17–22] When incorporating NPs in such nanocomposites, for the sake of property versatility one would desire a ligand with capabilities beyond just colloidal stabilization, i.e. a ligand with functionalities. Herein, we present the use of graphene quantum dots (GQDs) as ligands to stabilize nanoparticles.

GQDs can be viewed as a derivative of the extensively studied two-dimensional material graphene.[23–27] They are a class of nanometer-sized graphitic sheets with abundant edge functional groups.[28,29] Their size-related band gap and photoluminescence (PL) properties have permitted their application in bio-labeling.[29,30]

Recent incorporation of GQDs into nanocomposite materials also offers the opportunity to take advantage of their unique charge carrier extraction capability for better solar cell efficiency.[31,32] In this communication, we demonstrate that GQDs can be used directly as a native ligand exchanger and to also

[a]CAS Key Lab for Nanosystem and Hierarchy Fabrication, National Center for Nanoscience and Technology, Beijing, 100190, China. E-mail: lucg@nanoctr.cn; zytang@nanoctr.cn

[b]Key Laboratory of Synthesis and Natural Functional Molecular Chemistry of Ministry of Education, College of Chemistry & Materials Science, Northwest University, Xi'an, 710069, China. E-mail: xiegang@nwu.edu.cn

[c]Carbon Research Laboratory, Center for Nano Materials and Science, State Key Laboratory of Fine Chemicals, School of Chemical Engineering and Key Laboratory for Micro/Nano Technology of Liaoning Province, Dalian University of Technology, Dalian 116024, China

† Electronic supplementary information (ESI) available. See DOI: 10.1039/c5sc00910c
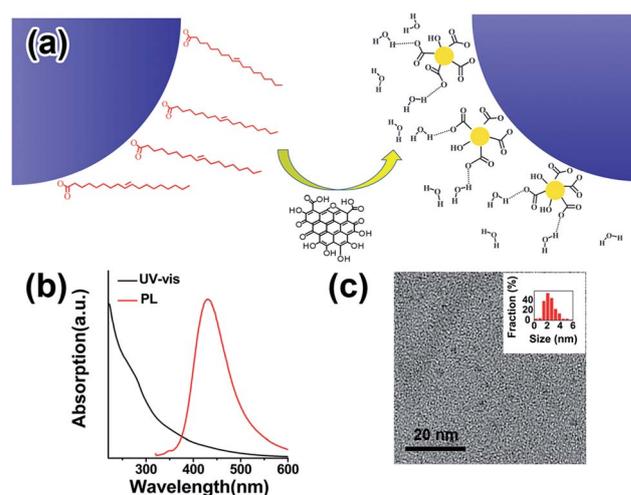
Fig. 1 (a) Schematic drawing of how GQDs may be used as capping ligands to replace native oleic acid ligands. (b) UV-vis and photoluminescence spectra of GQDs. (c) TEM image of GQDs; the inset presents the histogram of the size distribution of GQDs.

stabilize NPs in polar solvents (Fig. 1a).[33] We further show that, when the composite is made into a pellet by spark plasma sintering (SPS), the fusing of NPs is lessened and significantly enhanced thermoelectric performance is achieved, most likely due to the preservation of quantum confinement and carrier energy filtering.[34,35] This novel type of GQD ligand is thus advantageous over conventional molecular ligands when high temperature ligand stability is needed.

Results and discussion

Inorganic NPs were made following well-developed wet-chemistry methods.[36–39] For GQDs synthesis, graphene oxide (GO) from natural graphite powder was first prepared by a modified Hummer's method,[40] and a hydrothermal method was then adopted to cut the GO into small pieces of GQDs[41,42] (details in the ESI†). The as-synthesized GQDs are highly luminescent with a PL peak at 440 nm (Fig. 1b), while transmission electron microscopy (TEM) imaging shows the GQDs have a uniform size of around 2.5 nm (Fig. 1c), proving them to be of high quality. The ligand exchange processes were carried out in a nitrogen-filled glovebox. For a typical ligand exchange, 3 mL of NPs in toluene solution was added to 3 mL of GQDs in formamide and vigorously stirred for several hours. After complete phase transfer, the toluene phase was discarded, and the formamide phase was washed three times with fresh toluene. The resulting GQD–NPs were precipitated by acetone and finally redispersed in DMF or DMSO.

The insets in Fig. 2 and S1† present photographs of the NPs transferring from the non-polar phase (top phase) into the polar phase (bottom phase) with aid of the GQDs. The transfer starts upon contact of the GQD-containing polar phase with the NPs in toluene. Pb-based NPs are readily transferred within hours, while Cd-based NPs require a slightly longer time to accomplish the transfer, demonstrating the universality of GQDs as a phase transfer agent. This difference could be attributed to the different affinities of the surface cations (Pb *vs.* Cd) with GQDs. The TEM images before and after phase transfer indicate that the NPs' shape and size are preserved (Fig. 2). A thermogravimetric analysis shows that, as for 18 nm PbTe NPs, weight loss is 17% before GQD exchange and 8% after GQD exchange (Fig. S2†). By comparing the final residue weight of GQD–PbTe nanocomposites and that of pure GQDs, we estimate that the weight percentage of GQDs in this composite is about 14%.

The Fourier transform infrared spectroscopy (FTIR) spectrum of the NP dispersion after phase transfer shows a greatly reduced peak for the C–H stretching mode at ∼2900 cm^{-1} (Fig. 3a and S3†), confirming the removal of alkyl chains on the surface of the NPs. The peaks at 1670 cm^{-1} and 1590 cm^{-1} are assigned to the stretching modes of C=O and C=C, respectively, indicating the presence of GQDs after ligand exchange. Furthermore, ^{1}H nuclear magnetic resonance (NMR) spectroscopy clearly proves the exclusive removal of alkyl H atoms in the range of 0.8–2.5 ppm and alkene H atoms at 5.3 ppm (Fig. 3b and S4†); the chemical shifts at 3.6 ppm and 3.7 ppm of the GQD–NPs are assigned to the two types of H atoms on GQDs (Fig. S4†). This spectroscopic evidence is consistent with the proposed scheme (Fig. 1a) in which the native ligands of NPs are totally exchanged by GQDs after phase transfer.
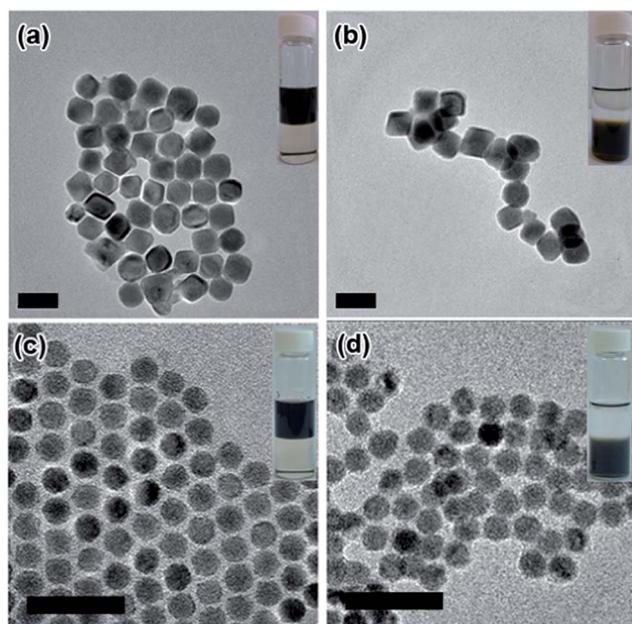

Fig. 2 TEM images of Pb-based NPs before (a and c) and after (b and d) GQD ligand exchange. (a and b) PbTe, 30 nm; (c and d) PbSe, 10 nm. The scale bars are 50 nm. Insets are photos of NPs dispersed in the (top) non-polar phase, toluene, and (bottom) the polar phase, formamide, with GQDs.
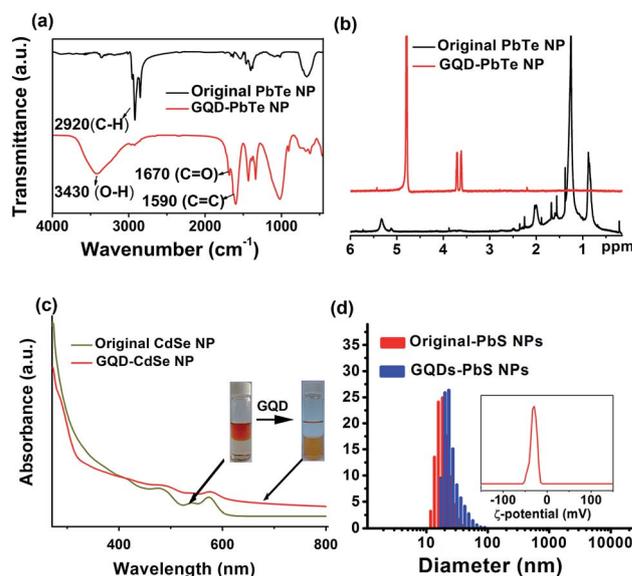

Fig. 3 (a) FTIR spectra and (b) ^{1}H NMR spectra of PbTe NPs before and after ligand exchange; (c) UV-vis spectra of CdSe NPs before and after ligand exchange. The first exciton peak of the NPs is preserved, while the GQD absorption feature near 287 nm is additionally observed. This indicates that the NP core structures are preserved during ligand exchange. (d) Size distribution of PbS NPs before (red) and after (blue) GQD ligand exchange; the inset shows the ζ-potential after GQD ligand exchange.

X-ray diffraction (XRD) patterns for PbTe NPs before and after GQD ligand exchange are shown in Fig. S5a.† Evidently, there is no observable change in the structural integrity for NPs during the phase transfer process. UV-vis spectroscopy of CdSe NPs before and after GQD ligand exchange further reveals no obvious shifting in the first exciton peak (Fig. 3c), and HRTEM imaging (Fig. S6†) also suggests no modification of the NP cores occurs upon GQD-coating.

It would be interesting to learn how the GQDs assemble near the surface of the NPs to form a stable dispersion in a polar solvent. We therefore performed a dynamic light scattering (DLS) study to reveal this behaviour *in situ*. Fig. 3d shows that the GQD–PbS NP complexes are dispersed in DMSO with a uniform hydrodynamic diameter slightly larger than that of the original NPs with organic ligands. This could be explained by the larger size of the solvation shells containing GQDs and polar solvent molecules compared to those containing the native oleic acid ligands. It should be noted that such shells collapse due to loss of solvent in the TEM chamber, resulting in the closer inter-NP distance shown in Fig. 2. All these complexes formed stable colloidal solutions and were stored at ambient conditions for more than 3 months without noticeable changes. The negatively charged surfaces (the negative ζ-potential in the insets of Fig. 3d and S5b†) suggest that the GQDs are grafted onto NP surfaces with some of their carboxylic groups, while the remaining carboxylic groups facing the polar solvent are deprotonated thus stabilizing the solvated NPs *via* increasing their energy of solvation. The proposed scenario is presented in Fig. 1a. It should be noted that the small size of GQDs limits us from obtaining more *in situ* details of their status in the GQD–NP complexes, which still remains a major challenge for almost all types of ligands on NP surfaces.

To further prove the binding of GQDs to NPs, we studied the PL of GQD-capped CdSe NPs dispersed in solution (Fig. 4).[43,44] CdSe NPs were selected because their emission is located in the visible range and easily measured. The PL intensity of GQDs after binding with the NPs is decreased by ∼90% (Fig. 4a), and the lifetimes for the two major decay branches are reduced from $\tau_1 = 1.34$ ns and $\tau_2 = 6.77$ ns to $\tau_1 = 0.98$ ns and $\tau_2 = 6.56$ ns, respectively (Fig. 4b), which suggests the occurrence of short

distance energy transfer from GQDs to CdSe NP cores. Meanwhile, the emission from CdSe NPs is almost completely quenched. We compared high resolution TEM images (Fig. S6†) for CdSe NPs before and after GQD ligand exchange and found no obvious change in their crystallinity, which indicates that the PL quenching of CdSe NPs is caused by poor surface trap passivation instead of core structural change. We suppose that passivation of CdSe NP surface traps with wide-band-gap shells such as ZnS would preserve the PL characteristics of CdSe NPs and allow us to better elucidate the energy transfer between GQDs and CdSe NPs. Such a detailed study is underway in our group to gain a deeper understanding of the energy flow in this composite material. The spectroscopy results indicate that GQDs are bound to the surface of the NPs and serve as ligands instead of free floating in the solution. Such interaction and energy transfer between GQD ligands and NP cores might also permit engineering of versatile properties into this type of composite, enabling progress toward functional materials.

Composites made from NPs are promising materials for thermoelectric applications, because of their inherent low thermal conductivity and enhanced Seebeck coefficients that result from quantum confinement and energy filtering effects.[35] However, NPs generally suffer from alloying and fusing at elevated temperatures, which weakens these effects and leads to an irreversibly decreased Seebeck coefficient.[45,46] By capping the PbTe NPs with GQDs, we demonstrate that thermally stable GQDs effectively lessen sintering of NPs in the composite. We made pellets (Fig. S7†) of GQD-capped (GQDs from coal oxidation, see ESI†) PbTe NPs by SPS for thermoelectric measurements. For comparison, control pellets were also prepared using PbTe NPs capped by the most common ligands, SCN anions, which decompose into gaseous species at the SPS temperature of 450 °C (ref. 3 and 47). Scanning electron microscopy (SEM) images of the cross sections of these two pellets reveal that much finer nanostructures exist in the pellets of GQD-capped NPs than those in SCN-capped NPs (Fig. 5a and b). The X-ray diffraction pattern also confirms that the PbTe crystalline domain size is smaller in the former composite (Fig. S8 and Table S1†). The presence of GQDs after SPS was confirmed by Raman spectroscopy (spectrum shown in Fig. S7b†), indicating its thermal stability. The above observations suggest that GQD-capping around PbTe NPs lessens their propensity to fuse together and maintains smaller crystalline domains. Such an effect leads to beneficial thermoelectric properties with enhanced Seebeck coefficients resulting from nanostructuring.

The thermoelectric measurements highlight the advantages of using GQDs over SCNs as capping agents for both electrical conductivity and Seebeck coefficient (Fig. 5c–f). The final calculated figure of merit (ZT) shows a peak value of 0.46 at 650 K for the GQD–PbTe NP complex, which is among the best for solution processed pure PbTe thermoelectric materials.[48–50] Numerically, the main reason for the good ZT is attributed to the enhanced n-type Seebeck coefficient at 650 K. The switching of conduction type from p to n for both pellets can be understood as the excitation of electrons in the composite at elevated temperature. Interestingly, the GQD-capped NP complex shows
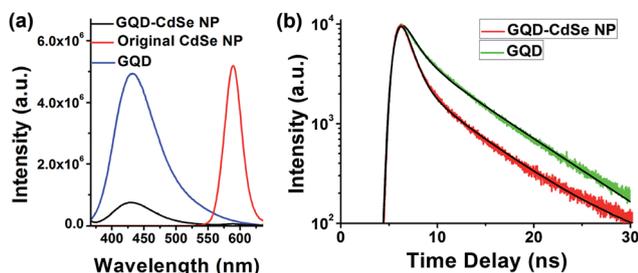

Fig. 4 (a) PL of GQDs alone (blue), CdSe NPs alone (red), and GQDs capping CdSe NPs (black), showing dramatically quenched emission for both CdSe NPs and GQDs in the composite. (b) Transient spectroscopy of GQD PL emission. For the two major decay branches, the lifetimes of GQDs alone are $\tau_1 = 1.34$ ns and $\tau_2 = 6.77$ ns, while the lifetimes of CdSe NPs with GQDs ligands are $\tau_1 = 0.98$ ns and $\tau_1 = 6.56$ ns.
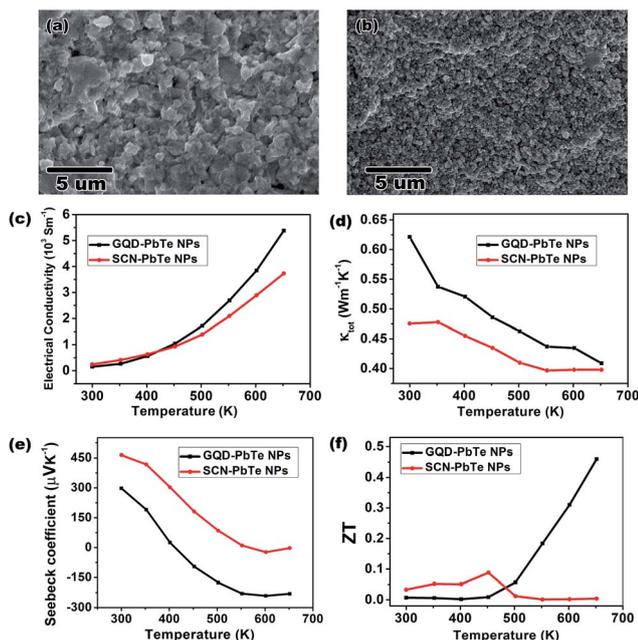
Fig. 5 The cross-section SEM images of pellets of SCN–PbTe NPs, (a), and GQD–PbTe NPs, (b) by SPS. The measured electrical conductivity, (c), thermal conductivity, (d), Seebeck coefficient, (e), and calculated ZT values, (f), are presented as functions of temperature.

Conclusions

In conclusion, for the first time, we reported the general capability of GQDs to serve as capping ligands exchanging native organic stabilizers for various types of semiconductor NPs. The FTIR, NMR, TEM and XRD characterization results proved that the ligand exchange is complete and that the integrity of the NPs is preserved. Thermoelectric measurement of GQD–PbTe composites revealed that the GQDs play a crucial role in limiting crystal size leading to an enhanced Seebeck coefficient, and thus a considerable ZT value of 0.46, without tuning the composition or doping level of the NPs. The PL lifetime of the GQD–NPs indicated efficient energy transfer between the GQD ligands and the NP cores. Given the many and yet tunable properties of GQDs, we anticipate that versatile properties could be engineered from this novel type of GQD–NP composite and to benefit various applications, including photovoltaic and thermoelectric devices, and catalysis.

Acknowledgements

a much quicker conduction-type switch and has a higher Seebeck coefficient value when a plateau is reached (Fig. 5e). The mechanisms to account for such enhanced Seebeck coefficient may be complicated. Besides the aforementioned quantum confinement effect, both electron doping and the carrier filtering effect of GQDs may also play a role, since a heterojunction is formed between the GQDs and the PbTe matrix. More detailed studies, therefore, are needed to understand the thermoelectric behaviour of the GQD–PbTe composite. Nevertheless, the GQD-capped NP complex shows a considerable ZT value even without tuning of composition and doping of the NPs,[51] which suggests the composite is a good candidate material for thermoelectric device fabrication. Given the thermal stability of GQDs, it is also advantageous over molecular capping ligands for controlling crystal size for optimized thermoelectric properties.

The prepared GQD–NP composite may also be applied when the collective properties of different components are desired. We have demonstrated the effect of GQDs in lessening the sintering of PbTe NPs for enhanced thermoelectric performance. Another application is likely to be photovoltaic materials. There are reports of mixing GQDs with TiO2 NPs[44,52] or ZnO nanowires[53] to improve solar cell performance by taking advantage of energy transfer between the GQDs and other nanomaterials. The tunable band structure of GQDs, together with their good interfacing with NPs, allows one to fine tune such energy transfer between GQDs and NPs in the hope of yielding a composite with novel properties, again superior to molecular ligands. Recent progress on large scale GQD production[26,54,55] will permit mass production of these GQD–NP composites for industrial applications.

Notes and references

1 F. J. Heiligtag and M. Niederberger, The Fascinating World of Nanoparticle Research, Mater. Today, 2013, 16, 262–271.
2 A. Nag, M. V. Kovalenko, J.-S. Lee, W. Liu, B. Spokoyny and D. V. Talapin, Metal-Free Inorganic Ligands for Colloidal Nanocrystals: S^{2-}, HS^-, Se^{2-}, HSe^-, Te^{2-}, HTe^-, TeS_3^{2-}, OH^-, and NH^{2-} as Surface Ligands, J. Am. Chem. Soc., 2011, 133, 10612–10620.
3 A. T. Fafarman, W.-K. Koh, B. T. Diroll, D. K. Kim, D.-K. Ko, S. J. Oh, X. Ye, V. Doan-Nguyen, M. R. Crump, D. C. Reifsnyder, C. B. Murray and C. R. Kagan, Thiocyanate-Capped Nanocrystal Colloids: Vibrational Reporter of Surface Chemistry and Solution-Based Route to Enhanced Coupling in Nanocrystal Solids, J. Am. Chem. Soc., 2011, 133, 15753–15761.
4 H. Zhang, B. Hu, L. Sun, R. Hovden, F. W. Wise, D. A. Muller and R. D. Robinson, Surfactant Ligand Removal and Rational Fabrication of Inorganically Connected Quantum Dots, Nano Lett., 2011, 11, 5356–5361.
5 J. J. Buckley, E. Couderc, M. J. Greaney, J. Munteanu, C. T. Riche, S. E. Bradforth and R. L. Brutchey, Chalcogenol Ligand Toolbox for CdSe Nanocrystals and Their Influence on Exciton Relaxation Pathways, ACS Nano, 2014, 8, 2512–2521.
6 M. V. Kovalenko, M. Scheele and D. V. Talapin, Colloidal Nanocrystals with Molecular Metal Chalcogenide Surface Ligands, Science, 2009, 324, 1417–1420.

7 A. Dong, X. Ye, J. Chen, Y. Kang, T. Gordon, J. M. Kikkawa and C. B. Murray, A Generalized Ligand-Exchange Strategy Enabling Sequential Surface Functionalization of Colloidal Nanocrystals, *J. Am. Chem. Soc.*, 2011, **133**, 998–1006.

8 E. L. Rosen, R. Buonsanti, A. Llordes, A. M. Sawvel, D. J. Milliron and B. A. Helms, Exceptionally Mild Reactive Stripping of Native Ligands from Nanocrystal Surfaces by Using Meerwein's Salt, *Angew. Chem., Int. Ed.*, 2012, **51**, 684–689.

9 A. Dong, Y. Jiao and D. J. Milliron, Electronically Coupled Nanocrystal Super lattice Films by *In Situ* Ligand Exchange at the Liquid–Air Interface, *ACS Nano*, 2013, **7**, 10978–10984.

10 M. H. Zarghami, Y. Liu, M. Gibbs, E. Gebremichael, C. Webster and M. Law, p-Type PbSe and PbS Quantum Dot Solids Prepared with Short-Chain Acids and Diacids, *ACS Nano*, 2010, **4**, 2475–2485.

11 Z. Deng, D. Cao, J. He, S. Lin, S. M. Lindsay and Y. Liu, Solution Synthesis of Ultrathin Single-Crystalline SnS Nanoribbons for Photodetectors *via* Phase Transition and Surface Processing, *ACS Nano*, 2012, **6**, 6197–6207.

12 B. Qin, Z. Zhao, R. Song, S. Shanbhag and Z. Tang, A Temperature-Driven Reversible Phase Transfer of 2-(Diethylamino)ethanethiol-Stabilized CdTe Nanoparticles, *Angew. Chem., Int. Ed.*, 2008, **47**, 9875–9878.

13 J. S. Owen, J. Park, P.-E. Trudeau and A. P. Alivisatos, Reaction Chemistry and Ligand Exchange at Cadmium–Selenide Nanocrystal Surfaces, *J. Am. Chem. Soc.*, 2008, **130**, 12279–12281.

14 J. M. Luther, M. Law, Q. Song, C. L. Perkins, M. C. Beard and A. J. Nozik, Structural, Optical, and Electrical Properties of Self-Assembled Films of PbSe Nanocrystals Treated with 1,2-Ethanedithiol, *ACS Nano*, 2008, **2**, 271–280.

15 L. Zhao and Z. Lin, Crafting Semiconductor Organic–Inorganic Nanocomposites *via* Placing Conjugated Polymers in Intimate Contact with Nanocrystals for Hybrid Solar Cells, *Adv. Mater.*, 2012, **24**, 4353–4368.

16 B. Ehrler, M. W. B. Wilson, A. Rao, R. H. Friend and N. C. Greenham, Singlet Exciton Fission-Sensitized Infrared Quantum Dot Solar Cells, *Nano Lett.*, 2012, **12**, 1053–1057.

17 X. Cao, Z. Yin and H. Zhang, Three-Dimensional Graphene Materials: Preparation, Structures and Application in Supercapacitors, *Energy Environ. Sci.*, 2014, **7**, 1850–1865.

18 D. J. Milliron, R. Buonsanti, A. Llordes and B. A. Helms, Constructing Functional Mesostructured Materials from Colloidal Nanocrystal Building Blocks, *Acc. Chem. Res.*, 2013, **47**, 236–246.

19 A. Llordes, G. Garcia, J. Gazquez and D. J. Milliron, Tunable Near-Infrared and Visible-Light Transmittance in Nanocrystal-in-Glass Composites, *Nature*, 2013, **500**, 323–326.

20 Y. Cheng, S. Lu, H. Zhang, C. V. Varanasi and J. Liu, Synergistic Effects from Graphene and Carbon Nanotubes Enable Flexible and Robust Electrodes for High-Performance Supercapacitors, *Nano Lett.*, 2012, **12**, 4206–4211.

21 Z. Mao, J. Guo, S. Bai, T.-L. Nguyen, H. Xia, Y. Huang, P. Mulvaney and D. Wang, Hydrogen-Bond-Selective Phase Transfer of Nanoparticles across Liquid/Gel Interfaces, *Angew. Chem., Int. Ed.*, 2009, **48**, 4953–4956.

22 C. Lu, A. Akey, W. Wang and I. P. Herman, Versatile Formation of CdSe Nanoparticle-Single Walled Carbon Nanotube Hybrid Structures, *J. Am. Chem. Soc.*, 2009, **131**, 3446–3447.

23 C. Tan, X. Huang and H. Zhang, Synthesis and Applications of Graphene-Based Noble Metal Nanostructures, *Mater. Today*, 2013, **16**, 29–36.

24 X. Huang, X. Qi, F. Boey and H. Zhang, Graphene-Based Composites, *Chem. Soc. Rev.*, 2012, **41**, 666–686.

25 X. Huang, Z. Yin, S. Wu, X. Qi, Q. He, Q. Zhang, Q. Yan, F. Boey and H. Zhang, Graphene-Based Materials: Synthesis, Characterization, Properties, and Applications, *Small*, 2011, **7**, 1876–1902.

26 C. Hu, C. Yu, M. Li, X. Wang, J. Yang, Z. Zhao, A. Eychmüller, Y. P. Sun and J. Qiu, Chemically Tailoring Coal to Fluorescent Carbon Dots with Tuned Size and Their Capacity for $Cu(II)$ Detection, *Small*, 2014, **10**, 4926–4933.

27 B. J. Schultz, C. J. Patridge, V. Lee, C. Jaye, P. S. Lysaght, C. Smith, J. Barnett, D. A. Fischer, D. Prendergast and S. Banerjee, Imaging local electronic corrugations and doped regions in graphene, *Nat. Commun.*, 2011, **2**, 372.

28 X. Yan, B. Li and L.-S. Li, Colloidal Graphene Quantum Dots with Well-Defined Structures, *Acc. Chem. Res.*, 2012, **46**, 2254–2262.

29 J. Shen, Y. Zhu, X. Yang and C. Li, Graphene Quantum Dots: Emergent Nanolights for Bioimaging, Sensors, Catalysis and Photovoltaic Devices, *Chem. Commun.*, 2012, **48**, 3686–3699.

30 J. Qian, D. Wang, F.-H. Cai, W. Xi, L. Peng, Z.-F. Zhu, H. He, M.-L. Hu and S. He, Observation of Multiphoton-Induced Fluorescence from Graphene Oxide Nanoparticles and Applications in *In Vivo* Functional Bioimaging, *Angew. Chem., Int. Ed.*, 2012, **51**, 10570–10575.

31 Z. Zhu, J. Ma, Z. Wang, C. Mu, Z. Fan, L. Du, Y. Bai, L. Fan, H. Yan, D. L. Phillips and S. Yang, Efficiency Enhancement of Perovskite Solar Cells through Fast ElectronExtraction: The Role of Graphene Quantum Dots, *J. Am. Chem. Soc.*, 2014, **136**, 3760–3763.

32 J. T.-W. Wang, J. M. Ball, E. M. Barea, A. Abate, J. A. Alexander-Webber, J. Huang, M. Saliba, I. Mora-Sero, J. Bisquert, H. J. Snaith and R. J. Nicholas, Low-Temperature Processed Electron Collection Layers of Graphene/TiO_2 Nanocomposites in Thin Film Perovskite Solar Cells, *Nano Lett.*, 2013, **14**, 724–730.

33 X. Yan, Q. Li and L.-S. Li, Formation and Stabilization of Palladium Nanoparticles on Colloidal Graphene Quantum Dots, *J. Am. Chem. Soc.*, 2012, **134**, 16095–16098.

34 M. Scheele, N. Oeschler, K. Meier, A. Kornowski, C. Klinke and H. Weller, Synthesis and Thermoelectric Characterization of Bi_2Te_3 Nanoparticles, *Adv. Funct. Mater.*, 2009, **19**, 3476–3483.

35 M. S. Dresselhaus, G. Chen, M. Y. Tang, R. G. Yang, H. Lee, D. Z. Wang, Z. F. Ren, J. P. Fleurial and P. Gogna, New

Directions for Low-Dimensional Thermoelectric Materials, *Adv. Mater.*, 2007, **19**, 1043–1053.

36 J. J. Urban, D. V. Talapin, E. V. Shevchenko and C. B. Murray, Self-Assembly of PbTe Quantum Dots into Nanocrystal Superlattices and Glassy Films, *J. Am. Chem. Soc.*, 2006, **128**, 3248–3255.

37 K.-S. Cho, D. V. Talapin, W. Gaschler and C. B. Murray, Designing PbSe Nanowires and Nanorings through Oriented Attachment of Nanoparticles, *J. Am. Chem. Soc.*, 2005, **127**, 7140–7147.

38 M. A. Hines and G. D. Scholes, Colloidal PbS Nanocrystals with Size-Tunable Near-Infrared Emission: Observation of Post-Synthesis Self-Narrowing of the Particle Size Distribution, *Adv. Mater.*, 2003, **15**, 1844–1849.

39 Z. A. Peng and X. Peng, Formation of High-Quality CdTe, CdSe, and CdS Nanocrystals Using CdO as Precursor, *J. Am. Chem. Soc.*, 2000, **123**, 183–184.

40 Y. Xu, H. Bai, G. Lu, C. Li and G. Shi, Flexible Graphene Films *via* the Filtration of Water-Soluble Noncovalent Functionalized Graphene Sheets, *J. Am. Chem. Soc.*, 2008, **130**, 5856–5857.

41 Q. Liu, B. Guo, Z. Rao, B. Zhang and J. R. Gong, Strong Two-Photon-Induced Fluorescence from Photostable, Biocompatible Nitrogen-Doped Graphene Quantum Dots for Cellular and Deep-Tissue Imaging, *Nano Lett.*, 2013, **13**, 2436–2441.

42 D. Pan, J. Zhang, Z. Li and M. Wu, Hydrothermal Route for Cutting Graphene Sheets into Blue-Luminescent Graphene Quantum Dots, *Adv. Mater.*, 2010, **22**, 734–738.

43 A. A. O. El-Ballouli, E. Alarousu, M. Bernardi, S. M. Aly, A. P. Lagrow, O. M. Bakr and O. F. Mohammed, Quantum Confinement-Tunable Ultrafast Charge Transfer at the PbS Quantum Dot and Phenyl-C_{61}-butyric Acid Methyl Ester Interface, *J. Am. Chem. Soc.*, 2014, **136**, 6952–6959.

44 K. J. Williams, C. A. Nelson, X. Yan, L. S. Li and X. Y. Zhu, Hot Electron Injection from Graphene Quantum Dots to TiO_2, *ACS Nano*, 2013, **7**, 1388–1394.

45 S. W. Finefrock, G. Q. Zhang, J. H. Bahk, H. Y. Fang, H. R. Yang, A. Shakouri and Y. Wu, Structure and Thermoelectric Properties of Spark Plasma Sintered Ultrathin PbTe Nanowires, *Nano Lett.*, 2014, **14**, 3466–3473.

46 M. Scheele, N. Oeschler, I. Veremchuk, S. O. Peters, A. Littig, A. Kornowski, C. Klinke and H. Weller, Thermoelectric Properties of Lead Chalcogenide Core–Shell Nanostructures, *ACS Nano*, 2011, **5**, 8541–8551.

47 T. Saraidarov, R. Reisfeld, A. Sashchiuk and E. Lifshitz, Synthesis and characterization of PbS nanocrystallites organized into different morphological assemblies, *J. Non-Cryst. Solids*, 2004, **345**, 698–702.

48 J. Dong, W. Liu, H. Li, X. Su, X. Tang and C. Uher, *In situ* synthesis and thermoelectric properties of PbTe–graphene nanocomposites by utilizing a facile and novel wet chemical method, *J. Mater. Chem. A*, 2013, **1**, 12503–12511.

49 M. Ibanez, R. Zamani, S. Gorsse, J. D. Fan, S. Ortega, D. Cadavid, J. R. Morante, J. Arbiol and A. Cabot, Core–Shell Nanoparticles As Building Blocks for the Bottom-Up Production of Functional Nanocomposites: PbTe-PbS Thermoelectric Properties, *ACS Nano*, 2013, **7**, 2573–2586.

50 M. V. Kovalenko, B. Spokoyny, J. S. Lee, M. Scheele, A. Weber, S. Perera, D. Landry and D. V. Talapin, Semiconductor Nanocrystals Functionalized with Antimony Telluride Zintl Ions for Nanostructured Thermoelectrics, *J. Am. Chem. Soc.*, 2010, **132**, 6686–6695.

51 M. Scheele, N. Oeschler, I. Veremchuk, K.-G. Reinsberg, A.-M. Kreuziger, A. Kornowski, J. Broekaert, C. Klinke and H. Weller, ZT Enhancement in Solution-Grown $Sb_{(2-x)}Bi_xTe_3$ Nanoplatelets, *ACS Nano*, 2010, **4**, 4283–4291.

52 S. Zhuo, M. Shao and S.-T. Lee, Upconversion and Downconversion Fluorescent Graphene Quantum Dots: Ultrasonic Preparation and Photocatalysis, *ACS Nano*, 2012, **6**, 1059–1064.

53 M. Dutta, S. Sarkar, T. Ghosh and D. Basak, ZnO/Graphene Quantum Dot Solid-State Solar Cell., *J. Phys. Chem. C*, 2012, **116**, 20127–20131.

54 R. Ye, C. Xiang, J. Lin, Z. Peng, K. Huang, Z. Yan, N. P. Cook, E. L. G. Samuel, C.-C. Hwang, G. Ruan, G. Ceriotti, A.-R. O. Raji, A. A. Martí and J. M. Tour, Coal As an Abundant Source of Graphene Quantum Dots, *Nat. Commun.*, 2013, **4**, 2943.

55 L. Wang, Y. Wang, T. Xu, H. Liao, C. Yao, Y. Liu, Z. Li, Z. Chen, D. Pan, L. Sun and M. Wu, Gram-scale synthesis of single-crystalline graphene quantum dots with superior optical properties, *Nat. Commun.*, 2014, **5**, 5357.